https://doi.org/10.33805/2641-7383.119
Volume 3 Issue 1 | PDF 119 | Pages 7

EDELWEISS PUBLICATIONS
OPEN ACCESS

Edelweiss Chemical Science Journal

Research Article ISSN: 2641-7383

Solid Polymer Electrolytes Derived from Oligomeric Poly(ethylene oxide) Chain-Grafted Crosslinked Polystyrene Microspheres

Wendy Zhao[1], Xinyi Mei[1], Zheng Yue[1] and Braja K Mandal[1*]

Affiliation: [1]Department of Chemistry, Illinois Institute of Technology, Chicago, USA

[*]Corresponding author: Braja K Mandal, Department of Chemistry, Illinois Institute of Technology, 3101 S. Dearborn St., Chicago, IL 60616, USA, E-mail: mandal@iit.edu

Citation: Zhao W, Mei X, Yue Z and Mandal BK. Solid polymer electrolytes derived from oligomeric poly(ethylene oxide) chain-grafted crosslinked polystyrene microspheres (2020) Edelweiss Chem Sci J 3: 17-23.

Received: Sep 28, 2020
Accepted: Nov 09, 2020
Published: Nov 13, 2020

Abstract

A new class of lithium-ion conducting Solid Polymer Electrolytes (SPEs) has been derived from oligomeric Polyethylene Oxide (PEO)-grafted Cross-linked Polystyrene (XPS) microspheres containing one or two lithium sulfonamide moieties. The SPE containing Li:O mole ratio of 1:8 displayed excellent ionic conductivity (in excess of 10^{-4}S/cm at 25°C) and good electrochemical stability (4.3 volts versus Li/Li^+). Thermal properties of these SPEs have also been investigated with Differential Scanning Calorimetry (DSC) and Thermogravimetric Analysis (TGA). These new SPEs possess amorphous character with a glass Transition Temperature (T_g) around 135°C, and no significant thermal decomposition until 420°C. Synthesis and characterization including surface morphologies of these SPEs are described.

Keywords: Lithium-ion batteries, Solid polymer electrolytes, Polymer-bound lithium salts, Ionic conductivity, Cyclic voltammetry, Optical microscopy.

Abbreviations: SPEs-Solid Polymer Electrolytes, PEO-Polyethylene Oxide, XPS- Cross-linked Polystyrene, DSC-Differential Scanning Calorimetry, TGA-Thermogravimetric Analysis, T_g-glass Transition Temperature, LiTFSI-Lithium bis(Trifluoromethane)Sulfonimide, EIS-Electrochemical Impedance Spectroscopy, CV-Cyclic Voltammetry, DIC-Differential Interference Contrast, FTIR-Fourier-Transform Infrared Spectroscopy, ESW-Electrochemical Stability Window

Introduction

The development of high energy density batteries with good safety and reliability has been an active area of research for the past three decades [1-5]. Advances in portable electronic devices, such as cell phones and laptops, have created a demand for smaller, lighter, yet more powerful energy sources. In particular, lithium-ion (Li-ion) batteries have received the most attention, due to the high redox potential of lithium and outstanding cycling stability [6,7]. Significant research has been focused on the development of electrolyte materials, which transport lithium ions between the electrodes. Although polar aprotic liquid electrolytes and gel polymer electrolytes containing 50-80% organic solvent can be used as the media for the transport of lithium ions, the requirement for bulky enclosures and the reported safety-related shortcomings make them less attractive for future applications [8-10]. Accordingly, several attempts have been made to develop SPEs that allow the use of complex shapes, greater ease of fabrication, free of leakage and much lower flammability.

In the past decades, numerous research studies have been concentrated on the PEO-based SPEs. PEO with C-O, C-C and C-H on the backbone has a good combination of chemical and electrochemical properties. PEO contains both crystalline and amorphous regions, and is very flexible (low glass transition temperature, T_g=-61°C). The most positive attribute of PEO-based SPEs is their high dissolution of lithium salts. The lithium ion conduction takes place in the amorphous phases of PEO via diffusion, and the lithium ion migration associated with segmental mobility of the PEO chains. The major drawback of PEO-based SPEs is their poor room temperature ionic conductivity due to the high crystallinity of PEO-lithium salt complex. Thus far, no SPE is known that efficiently transports lithium ions at conductivities in excess of $10^{-3}Scm^{-1}$ at 25°C, which is considered commercially viable [11-14].

Recently, polymer microspheres, such as XPS beads, have attracted a great deal of interest in developing new materials due to their special particle morphologies and characteristics, such as large specific surface area, remarkable aggregation effects, and surface reaction capability [15-18]. Thus, XPS beads can act as building blocks in construction of new micro-structured hybrid systems, owing to their ease of chemical modification [19-23]. In this study, we have synthesized and examined two SPEs (SPE-A1 and SPE-A2), in which XPS beads are grafted with oligomeric PEO chains through a sulfonamide moiety containing one or two lithium ions [24-26]. The motivation for such a molecular design originated from the fact that lithium ions can be transported easily in this hybrid system by introducing a large number of highly flexible pendant PEO oligomeric chains on the outer surface of XPS

beads (**Figure 1**). Such a structural modification would provide ideal Li^+ conducting pathways at the XPS particle surface, leading to superior ionic transport [27,28]. The presence of numerous oligoether short chains on the peripheral surface of the XPS will allow faster ion mobility compared with a linear coil having the same molecular weight. This is because, in a given polymer, the chain end is more flexible than the chain middle [29]. Moreover, covalently-linked lithium sulfonamide moieties provide a secondary source of lithium ions, leading to superior ionic transport properties. Additionally, the thermal stability of the SPE is expected to improve due to the presence of XPS beads in the SPE.

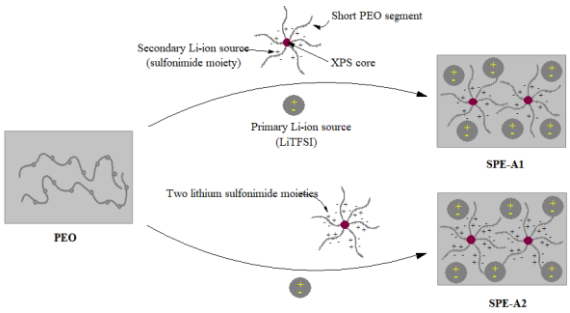

Figure 1: Schematic of the proposed SPEs.

Experimental

Materials

Commercially available chlorosulfonated XPS, XPS-SO_2Cl, with diameters near 128µ, was provided by Biotage LLC, NC. 3-Nitrobenzenesulfonyl chloride was obtained from Sigma-Aldrich Chemicals, MO. Zinc dust, commercial grade (total zinc 98.5%), was obtained from U.S. Zinc®, TX, and used as received. Di-ammonium hydrogen phosphite was purchased from MP Biomedicals LLC, OH. Lithium bis(trifluoromethane)Sulfonimide (LiTFSI) was obtained from 3M, MN. The monoamine-terminated oligomeric PEOs, Jeffamine® M-600 (Mw 600, PO/EO 9/1) and M-1000 (Mw 1,000, PO/EO 3/19), were received as gift samples from Huntsman Corporation, TX.

Synthesis of XPS-Li-PEO

2g of XPS-SO_2Cl, 9g of Jeffamine® M-1,000 (or 6g of Jeffamine® M-600) and 25 mL of dry THF were placed in a three-necked round bottom flask (50mL) connected with a reflux condenser. After 5 min, 2 mL of triethylamine, diluted with 10mL of dry THF, was added slowly to the mixture under stirring through a dropping funnel. The reaction was conducted under argon in an ice water bath for the initial 2 hours and subsequently stirred at room temperatures overnight. The sulfonamide product was filtered using a sintered funnel and washed with 20mL of water, 20mL of methanol, and then 10mL of acetone. The product was dried under vacuum for 24 hours prior to the lithiation reaction, which was performed by stirring overnight the product with an excess of 1M LiOH solution. XPS-Li-PEO was isolated by filtration followed by the aforementioned sequence of the washing protocol.

Synthesis of XPS-Li_2-PEO

Nitro Derivative: 2.5g (0.011mol) of 3-nitrobenzenesulfonyl chloride, 15g (0.015mol) of Jeffamine® M-1,000 (or 8.8g of Jeffamine® M-600) and 50mL of methylene chloride were mixed in a 100mL three-necked round bottom flask, which was set in an ice bath and equipped with a dropping funnel. 1mL of triethylamine diluted with 10mL of methylene chloride was added drop-wise to the mixture. The reaction was continued overnight under argon at room temperature. After the reaction, $HNEt_3Cl$ was filtered off and the filtrate was transferred into a 100mL flask, and 50mL of ether was added to yield more $HNEt_3Cl$, which was filtered off. The filtrate was transferred to a flask with 50 mL of hexane and kept in the freezer overnight, with the formation of two layers. Excess Jeffamine® was removed by decanting the hexane layer. This freezing-decantation procedure was repeated three times to obtain the pure nitro derivative. Yield: 6.97g (62%).

Amino Derivative: The aforementioned nitro compound, 2g (2.55 mmol), and commercial grade zinc dust, 0.2g (3.05mmol), in methanol (2mL) were stirred with 0.68g (5.07mmol) of di-ammonium hydrogen phosphite at room temperature. After 45 min, reaction was complete, monitored by TLC (silica plate chloroform/methanol=90/10, v/v). The mixture was filtered to remove residual zinc dust. The organic layer was evaporated and the residue dissolved in 10mL of methylene chloride and washed with saturated sodium chloride solution to remove ammonium formate. The organic layer was evaporated in a rotovap and the product dried under high vacuum to obtain the amino compound. Yield: 1.52g (76%). 1H-NMR (300MHz, $CDCl_3$): δ (ppm): 1.09 (polyether CH_3), 3.20-3.40 (polyether CH_2), 3.50 (polyether CH), 3.45 (polyether CH_3), 7.50-8.50 (aromatic CH), 6.28 (aromatic NH_2) and 6.45 (sulfonamide NH).

XPS-Li_2-PEO: The synthesis of the bis-sulfonamide derivative and the subsequent lithiation reaction were performed according to the procedure described earlier for XPS-Li-PEO, using 2g of XPS-SO_2Cl and 9g of the aforementioned amino derivative.

Preparation of SPE Film

Ten different polymer electrolyte films with varied compositions were prepared (**Table 1**). The SPE-A was based on Jeffamine® M-1000. SPE-B was based on Jeffamine® M-600; A1 and B1 contain a single lithium sulfonamide group per repeat unit, while A2 and B2 contain two lithium sulfonamide groups per repeat unit. The primary source of lithium ions was attributed to LiTFSI. The ratios of Li:O (lithium ion per ethylene oxide moieties) were varied from 1:6 to 1:12 (Table 1). Only 3.5% by weight of PEO (Mw=4,000,000) from Sigma-Aldrich was added to each formulation to obtain free-standing thin films (~0.150mm).

The traditional solvent casting method was employed to cast thin films [30-32]. The components for each sample were dissolved in acetonitrile in a round bottom flask, then poured into a beaker and kept at 60°C under vacuum to remove solvent. The resulting film was placed between two PTFE coated sheets and hot-pressed (100°C, 500 psi, 30 seconds). The film thickness was controlled using two thin steel plates as spacers.

Sample ID	Composition	LiTFSI Content
PEO/1:12 (Control-1)	PEO	Li:O/1:12
PEO/1:8 (Control-2)	PEO	Li:O/1:8
SPE-A1/1:12	1000 M-Li-XPS with 10% PEO	Li:O/1:12
SPE-A1/1:8	1000 M-Li-XPS with 10% PEO	Li:O/1:8
SPE-A1/1:7	1000 M-Li-XPS with 10% PEO	Li:O/1:7
SPE-A1/1:6	1000 M-Li-XPS with 10% PEO	Li:O/1:6
SPE-A2/1:12	1000 M-(Li)2-XPS with 10% PEO	Li:O/1:12
SPE-A2/1:8	1000 M-(Li)2-XPS with 10% PEO	Li:O/1:8
SPE-B1/1:8	600 M-Li-XPS with 10% PEO	Li:O/1:8
SPE-B2/1:8	600 M-(Li)2-XPS with 10% PEO	Li:O/1:8

Table 1: Compositions of SPE films.

Ionic Conductivity

The ionic conductivities of the electrolytes were measured using Electrochemical Impedance Spectroscopy (EIS). The SPE films were cut into a circle and placed between two steel electrodes and subjected to an impedance analyzer [30-32]. Ionic conductivities were measured with all ten SPE films at temperatures ranging from 25°C to 70°C. A Solartron® model SI-1287 electrochemical interface coupled to a

Solartron® model-1260 frequency response analyzer was used to obtain the EIS measurements. The bulk resistance was determined from the high frequency intercept of the real axis of the complex impedance plot. The conductivity was calculated using the equation σ=I/RbA, where I is the thickness, A is the area of the testing films, and Rb is the measured bulk resistance.

Cyclic Voltammetry

The electrochemical stability of a representative sample SPE-A2 was measured by Cyclic Voltammetry (CV) using a Hohsen electrochemical test cell, with a stainless steel working electrode and lithium film counter/reference electrode, while the solid polymer electrolyte was placed between working and counter/reference electrodes [30-32]. All the preparation steps were carried out in side an Argon filled glove box. CV is performed with a computer controlled Solartron® 1287 Electrochemical Interface, employing the Corrware™ software. The experiments were performed by applying a voltage sweep from 2V to 5V at a scan rate of 10 mV/s on cells that are thermally equilibrated at 25°C for at least 1 hour.

Differential Scanning Calorimetry Measurements

The Differential Scanning Calorimetry (DSC) measurement of representative sample, SPE-A2/1:8 was conducted and compared with a reference (control-2) polymer electrolyte, using Seiko DSC 220C. The scanning was performed from 25°C to 200°C to observe the changes in thermal properties of the polymer electrolytes. DSC scanning cycles included equilibration at 25°C, ramp 10°C per minute to 200°C, mark end of cycle 0, isothermal for 5.0 minutes, ramp 10°C per minute to 25°C, mark end of cycle 0 [30,31].

Thermogravimetric Analysis Measurements

The thermal stability of representative sample, SPE-A2/1:8 and the reference sample, control-2 was measured by TGA, using TG/DTA 6200 system. Sample was heated in the analyzer from 25ºC to 500ºC at a heating rate of 10°C per minute under inert atmosphere [30-32].

Film Images by Fluorescence Microscope

Optical images of the best polymer electrolyte film (SPE-A2/1:8) were obtained by using an Olympus Fluorescence/ Differential Interference Contrast (DIC) Analytical Digital Microscope and ColorView soft imaging system with objectives of UMPlanFI 5X/0.15, UMPlanFI 20X/0.46 and UMPlanFI 50X/0.80 and filters, U-AN 360-3 and U-P03.

Results and Discussion

Synthesis of PEO-Grafted XPS (XPS-Li_x-PEO)

Figure 2 depicts the general methodology for the preparation of XPS-Li-PEO in two steps starting from commercially available XPS-SO_2Cl. The first step involves reaction with an excess polyetheramines (Jeffamines®, Mw 600 or 1000) in the presence of triethylamine to produce sulfonamide derivatives. In the second step, the XPS-Li-PEO derivatives were obtained by treating sulfonamide derivatives with LiOH. The structures of both the intermediate and the final product were confirmed by the FTIR spectroscopy (Fourier-Transform Infrared Spectroscopy). The spectrum of the amide compound showed these signature characteristic peaks: 1368 and 1165 cm^{-1} (sulfonyl), 3324, 1601, and 758 cm^{-1} (amide N-H), 2983 and 1470, cm^{-1} (aliphatic C-H) and 1030 and 608 cm^{-1} (C-O-C). The signature peaks for XPS-Li-PEO appeared at: 1377 and 1172 cm^{-1} (sulfonyl), 3003 and 1450 cm^{-1} (aliphatic C-H), 1082 and 578 cm^{-1} (C-O-C).

For the preparation of PEO-Li_2-XPS (**Figure 3**), first the polyetheramines (Jeffamines®, Mw 600 or 1000) were treated with 3-nitrobenzenesulfonyl chloride. The resulting nitro derivative was reduced to the corresponding amino compound using a mild procedure involving zinc-dust and di-ammonium hydrogen phosphite [33,34]. Once the amino compound was obtained, then PEO-Li_2-XPS was conveniently prepared following the strategy established for PEO-Li-XPS. The structures of the intermediates and the final product were confirmed by the FTIR spectroscopy. The IR spectrum (Infrared Spectrum) of the polyether tethered 3-nitro sulfonamide compound showed the signature peaks at 1535 and 1380 cm^{-1} for aromatic nitro group. The spectrum of the polyether tethered 3-amino sulfonamide compound showed a doublet for the primary aromatic amine at 3459 and 3382 cm^{-1}. Other characteristic peaks include 1375 and 1117 cm^{-1} (sulfonyl), 1605 and 782 cm^{-1} (amide N-H), 2967 and 1463 cm^{-1} (aliphatic C-H) and 1256 and 523 cm^{-1} (C-O-C). The structure of the amino compound was also confirmed by 1H-NMR (300 MHz, $CDCl_3$).

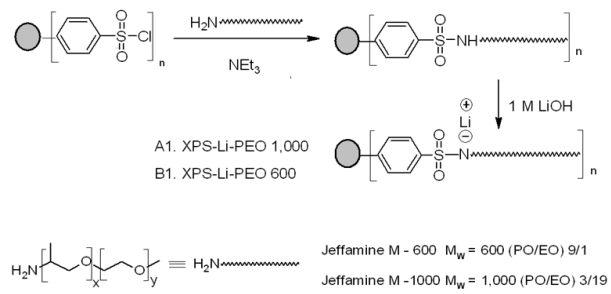

Figure 2: Synthesis of XPS-Li-PEO.

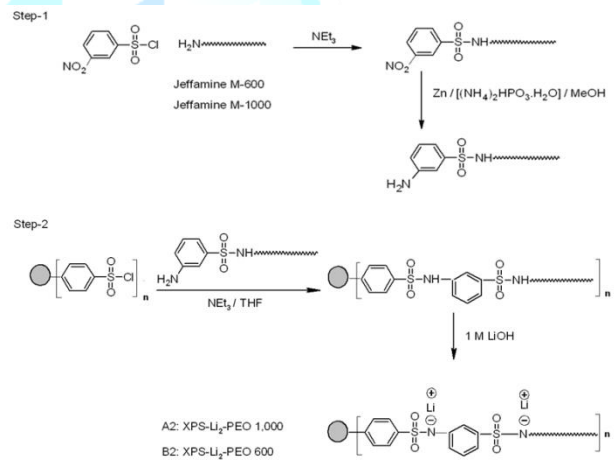

Figure 3: Synthesis of XPS-Li_2-PEO.

Characterization of SPEs

Ionic conductivity: Ionic conductivities were measured with all SPE complexes containing LiTFSI (Li/O ratio: 1/12-1/6) and 2-5 wt.% PEO (M_w=400,000) to improve the flexibility of the free-standing thin SPE films (0.12-0.15mm). The ionic conductivities of XPS-Li_x-PEO SPE, along with a standard PEO SPE (control-1 and 2 in Table 1), are shown as Arrhenius plots in **Figure 4a-Figure 4d**. Compared with the standard PEO SPE, the new SPEs provided higher ionic conductivity in the temperatures range of 25°C to 70°C (**Figure 4a, Figure 4b**). The ionic conductivity increases with the increase of the number of lithium sulfonamide groups and the polyetheramine segment with more ethylene oxide repeat units (such as Jeffamine® M-1000 (PO/EO 3/19)). The SPE with Jeffamine® M-600 (PO/EO 9/1) displayed lower ionic conductivity. The highest ionic conductivity was obtained with the film assigned as SPE-A2/1:8: 1.87 x 10^{-4}S/cm at 25°C and 5.05 x 10^{-3}S/cm at 70°C. This SPE was synthesized with Jeffamine® M-1000 in conjunction with two sulfonamide groups (**Figure 4c**).

Figure 4d shows the ionic conductivity of the SPE-A1 with 4 different loading levels of LiTFSI in the Li:O ratios of 1:12, 1:8, 1:7 and 1:6. Results indicate that the ionic conductivity of SPE with Li:O ratio of 1:8 is much higher than 1:12. However, this trend was not followed by continually increasing the amount of the salt in the samples with Li:O ratio of 1:7 and 1:6. In fact, after the conductivity reaches to the maximum point at the composition with Li:O ratio of 1:8, the addition of excess lithium salt does not continue to increase the ionic conductivity. This has been explained that as the salt is increased above an optimum concentration, the distance between ions becomes significant smaller, the ions become closer to one another and tend to associate to form ion aggregates or ion clusters in the matrix; which could reduce the number of free-ions and restrict the chain segment mobility, leading to low ionic conductivity [35-37].

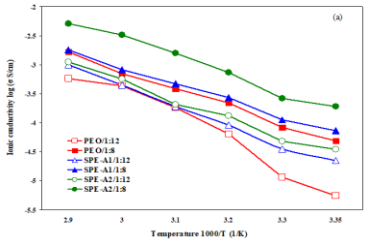

Figure 4a: Ionic conductivities; New SPEs vs. Control.

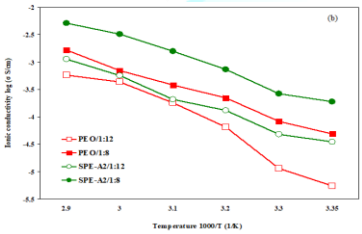

Figure 4b: SPE-A2 (1000 M-Li_2-XPS) vs. Control.

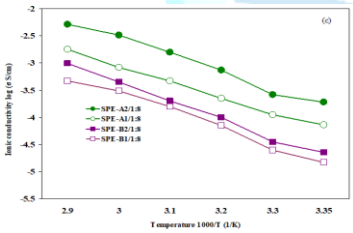

Figure 4c: SPE-A (M-1000 derivative) vs. SPE-B (M-600 derivative) in two compositions, XPS-Li_2-PEO and XPS-Li-PEO.

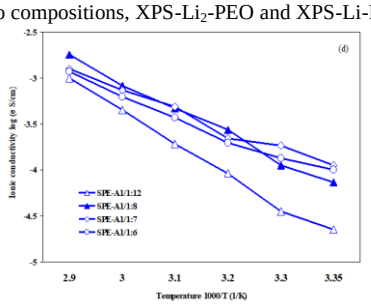

Figure 4d: Evaluation of LiTFSI loading level on SPE-A1.

Electrochemical stability: Electrochemical Stability Window (ESW) is one of the most important parameters for the electrolytes used in electrochemical cells. The ESW of the electrolyte, defined as the voltage range between which the SPE is neither oxidized nor reduced, is usually measured by the CV experiment. As shown in **Figure 5**, the PEO-Li_2-XPS SPE displayed good electrochemical stability. The representative film comprised of SPE-A2/1:8, was subjected to an applied field of 2 to 5 volts versus Li/Li^+. No oxidation or reduction peak in the voltage window of 2.5 to 4.3 volts was observed. The oxidation peak which is ascribed to the breakdown of PEO-Li_2-XPS system was not appeared until 4.3 Volts versus Li/Li^+ [38,39].

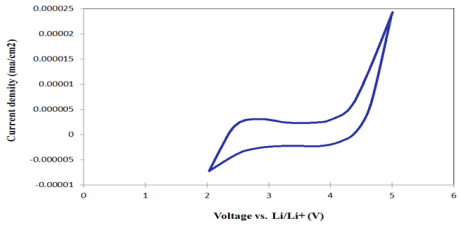

Figure 5: Cyclic Voltammogram of SPE-A2/1:8 film.

Differential scanning calorimetry: The DSC curves of the two films, PEO-$(Li)_2$-XPS (curve-a), and PEO control (curve-b) are shown in **Figure 6**. Curve-b shows a sharp endothermic peak observed at 54°C which corresponds to the crystalline melting Temperature (T_m) of the pure PEO electrolyte. By contrast, there was no heat flow feature in curve-a until an endothermic baseline shift occurred at 135°C, corresponding to the glass transition temperature (T_g) of the PEO-$(Li)_2$-XPS. The result indicates that this new polymer composite, PEO-$(Li)_2$-XPS, is an amorphous material, i.e., substantially free of crystalline phases. The microspheres in the system aided in suppressing the crystallinity of the polymer electrolyte [40]. The large surface area of microspheres could prevent the local PEO chain reorganization, with the result of a high degree of disorder. Similar to the polymer composite incorporated with inorganic particles or fillers [41-43], we believe that the XPS beads destroyed the crystallinity of the PEO, thus making charge transfer much easier in the amorphous polymer network. In addition, the desired high T_g overcomes the deficiencies of poor thermal stability of PEO, associable with the high crystallinity and low glass transition temperature (-61°C) of PEO.

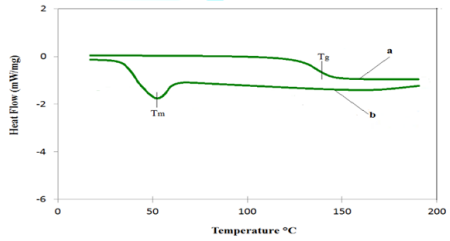

Figure 6: DSC traces of PEO-$(Li)_2$-XPS and PEO Control.

Thermogravimetric analysis: Figure 7 shows the TGA curves of XPS-Li_2-PEO versus PEO control-2. The PEO (curve-b) decomposed at the temperature range 200-415°C with total weight loss of 99.66%. Unlike the pure PEO, the XPS-Li_2-PEO (curve-a) underwent a three-step thermal degradation process. The first weight loss of 16.32% at the temperature range about 150-200°C is attributed to chain decomposition of polyetheramine (Jeffamine®), and the second weight loss of 12.27% at about 300-350°C is attributed to chain decomposition of the PEO. The final 61.52% weight loss of the XPS-Li_2-PEO composite occurred at the temperature range about 420-460°C, which is visibly higher than the decomposition temperature of the pure PEO [43]. As seen from the Figure 7, the major decomposition of the XPS-Li_2-PEO electrolyte does not occur until 420°C.

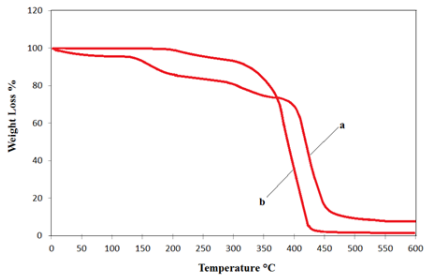

Figure 7: TGA curves of XPS-$(Li)_2$-PEO and PEO Control.

The electrolyte sample that showed the best ionic conductivity, XPS-Li_2-PEO was evaluated for surface image by Fluorescence/DIC Microscopy. Four digital photographs were taken to describe the morphology of this SPE material (**Figure 8**). In these images, the XPS beads were dispersed in a continuous phase to form an ideal matrix for the polymer electrolyte. **Figure 8a** reveals that the XPS particles are spherical with a perfectly round shape. **Figure 8b** shows the light-colored material covering the XPS beads. This indicates that the XPS microspheres were grafted by oligomeric poly(ethylene oxide) and polysulfonamide derivatives. **Figure 8c** depicts the phase contrast ratio of the XPS beads and the grafted PEO to be approximately 50/50 in the electrolyte matrix. **Figure 8d** shows the surface profile of the film, which shows a smooth, free of defects and well-connected network. Presumably, there are numerous pathways around on the surface of the XSP spheres. It turns out that this morphology is favorable for enhanced three-dimensional ion transport across the film.

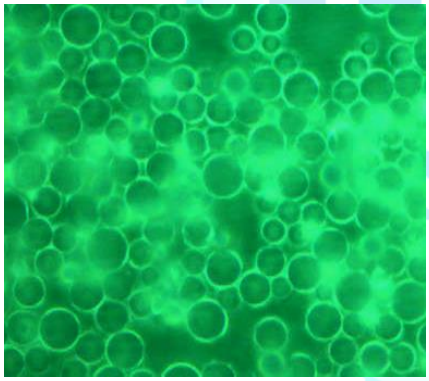

Figure 8a: Fluorescence/DIC Microscopy digital photographs of XPS-Li_x-PEO film, 20X, transmitted light source with filter.

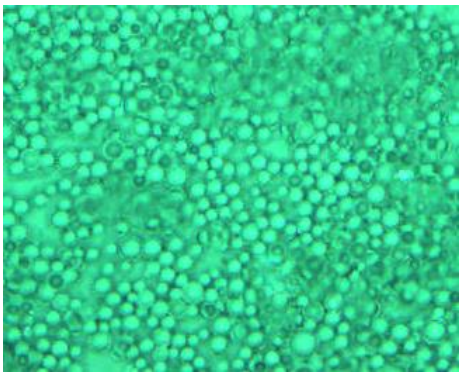

Figure 8b: 5X, reflect light source with filter.

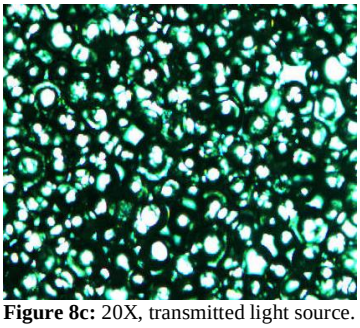

Figure 8c: 20X, transmitted light source.

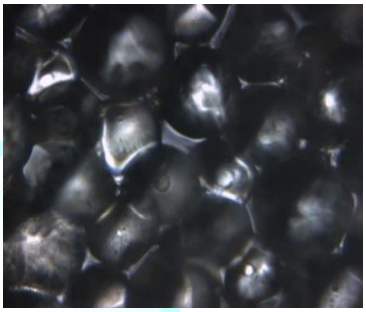

Figure 8d: 50X, reflect light source.

Conclusion

In conclusion, we have designed and synthesized two classes of new ion-conductive SPE composites, which contain oligomeric PEO-grafted XPS microspheres containing 1-2 lithium sulfonamide moieties. The grafted lithium sulfonamide moieties provide a secondary source of lithium ions that improved ionic conductivity. The SPE film containing LiTFSI in the Li:O mole ratio of 1:8 displayed excellent ionic conductivity ($1.87 \times 10^{-4} Scm^{-1}$ at $25^{\circ}C$, $5.05 \times 10^{-3} S\ cm^{-1}$ at $70^{\circ}C$), including good electrochemical stability window up to 4.3 volts versus Li/Li^{+}. DSC and TGA results reveal that the new SPE is an amorphous material with a T_g of $135^{\circ}C$, and thermal decomposition temperature of $430^{\circ}C$ due to the incorporation of XPS beads which destroyed crystallinity and improved thermal stability. Morphology images of ideal surface profile were observed, which is favorable for superior lithium ion transport. Overall, these materials displayed good ionic conductivity, electrochemical stability and thermal properties, resulting in improved performance when compared with the standard LiTFSI-based PEO electrolytes. Thus, such materials may have potential for the development of high energy density rechargeable lithium batteries.

References

1. Chen X, Shen W, Vo TT, Cao Z and Kapoor A. An overview of lithium-ion batteries for electric vehicles (2012) 2012 10th International Power and Energy Conference (IPEC), Vietnam pp-230-235. https://doi.org/10.1109/asscc.2012.6523269
2. Shen X, Liu H, Cheng X-B, Yan C and Huang J-Q. Beyond lithium ion batteries: Higher energy density battery systems based on lithium metal anodes (2018) Ener Stor Mater 12: 161-175. https://doi.org/10.1016/j.ensm.2017.12.002
3. Yin Y, Wan L and Guo Y. Silicon-based nanomaterials for lithium-ion batteries (2012) Chinese Sci Bull 57: 4104-4110. https://doi.org/10.1007/s11434-012-5017-2

4. Fotouhi A, Auger DJ, Propp K, Longo S and Wild M. A review on electric vehicle battery modelling: From Lithium-ion toward Lithium-Sulphur (2016) Ren Sus Ener Rev 56: 1008-1021. https://doi.org/10.1016/j.rser.2015.12.009
5. Choi JW and Aurbach D. Promise and reality of post-lithium-ion batteries with high energy densities (2016) Nat Rev Mater 1: 16013. https://doi.org/10.1038/natrevmats.2016.13
6. Korthauer R. Lithium-Ion Batteries: Basics and Applications (2018) Springer International Publishing, Germany.
7. Zhang Z and Zhang SS. Rechargeable Batteries (2015) Springer International Publishing, Germany.
8. Barnett B, Ofer D, Sriramulu S and Stringfellow R. Lithium-Ion Batteries lithium-ion battery , Safety lithium-ion battery safety (2012) Springer New York, USA pp 6097-6122.
9. Doughty DH and Roth EP. A General discussion of Li ion battery safety (2012) Interface Mag 21: 37-44.
10. Lu D, Shao Y, Lozano T, Bennett WD, Graff GL, et al. Failure mechanism for fast-charged lithium metal batteries with liquid electrolytes (2015) Adv Energy Mater 5: 1400993. https://doi.org/10.1002/aenm.201400993
11. Yue L, Ma J, Zhang J, Zhao J, Dong S, et al. All solid-state polymer electrolytes for high-performance lithium ion batteries (2016) Ener Stor Mater 5: 139-164. https://doi.org/10.1016/j.ensm.2016.07.003
12. Xue Z, He D and Xie X. Poly(ethylene oxide)-based electrolytes for lithium-ion batteries (2015) J Mater Chem A 3: 19218-19253. https://doi.org/10.1039/c5ta03471j
13. Cui M and Lee PS. Solid polymer electrolyte with high ionic conductivity via layer-by-layer deposition (2016) Chem Mater 28: 2934-2940.
14. Ngai KS, Ramesh S, Ramesh K and Juan JC. A review of polymer electrolytes: fundamental, approaches and applications (2016) Ionics (Kiel) 22: 1259-1279. https://doi.org/10.1007/s11581-016-1756-4
15. Šálek P, Horák D and Hromádková J. Novel preparation of monodisperse poly(styrene-co-divinylbenzene) microspheres by controlled dispersion polymerization (2018) Polym Sci Ser B 60:9-15. https://doi.org/10.1134/s1560090418010116
16. Chang Z, Zhang DS, Chen Q and Bu XH. Microporous organic polymers for gas storage and separation applications (2013) Phys Chem Chem Phys 15: 5430-5442. https://doi.org/10.1039/c3cp50517k
17. Chopade SA, Au JG, Li Z, Schimdt PW, Hillmyer MA, et al. Robust polymer electrolyte membranes with high ambient-temperature lithium-ion conductivity via polymerization-induced microphase separation (2017) ACS Appl Mater Interfaces 9: 14561-14565. https://doi.org/10.1021/acsami.7b02514
18. Albuszis M, Roth PJ, Exnowitz F, Wong DC, Pauer W, et al. Synthesis and in-depth characterization of reactive, uniform, crosslinked microparticles based on free radical copolymerization of 4-vinylbenzyl azide (2016) Polym Chem 7: 1168-1180. https://doi.org/10.1039/c5py01848j
19. Prasanth R, Aravindan V and Srinivasan M. Novel polymer electrolyte based on cob-web electrospun multi component polymer blend of polyacrylonitrile/poly(methyl methacrylate)/polystyrene for lithium ion batteries- Preparation and electrochemical characterization (2012) J Power Sources 202: 299-307. https://doi.org/10.1016/j.jpowsour.2011.11.057
20. Cong M, Chen T, Cai W, Li H, Cong M, et al. Controlled growth of metal nanoparticles on amino-functionalized polystyrene microspheres and their application in surface-enhanced Raman spectroscopy (2013) Mater Chem Phys 142: 756-762. https://doi.org/10.1016/j.matchemphys.2013.08.040
21. Li CP, Wang JQ, Shi Y, Liu Z, Lin J, et al Controlled synthesis of branched polystyrene via RAFT technique in the presence of chain transfer monomer p-vinyl benzene sulfonyl chloride (2012) Macromol Res 20: 858-867. https://doi.org/10.1007/s13233-012-0126-y
22. Rozik NN, Yakoob J, Saad E and Abdelmesseh SL. Mechanical and electrical properties of acrylonitrile butadiene rubber filled with waste carbon (2017) KGK Kautschuk Gummi Kunststoffe 70: 30-35.
23. Ozer O, Ince A, Karagoz B and Bicak N. Crosslinked PS-DVB microspheres with sulfonated polystyrene brushes as new generation of ion exchange resins (2013) Desalination 309: 141-147. https://doi.org/10.1016/j.desal.2012.09.024
24. Bouchet R, Maria S, Meziane R, Aboulaich A, Lienafa L, et al. Single-ion BAB triblock copolymers as highly efficient electrolytes for lithium-metal batteries (2013) Nat Mater 12: 452-457. https://doi.org/10.1038/nmat3602
25. Lu Q, Fang J, Yang J, Yan G, Liu S, et al. A novel solid composite polymer electrolyte based on poly(ethylene oxide) segmented polysulfone copolymers for rechargeable lithium batteries (2013) J Memb Sci 426: 105-112. https://doi.org/10.1016/j.memsci.2012.09.038
26. Khurana R, Schaefer JL, Archer LA and Coates GW. Suppression of lithium dendrite growth using cross-linked polyethylene/poly(ethylene oxide) electrolytes: A new approach for practical lithium-metal polymer batteries (2014) J Am Chem Soc 136: 7395-7402. https://doi.org/10.1021/ja502133j
27. Ibrahim S, Ahmad R and Johan MR. Conductivity and optical studies of plasticized solid polymer electrolytes doped with carbon nanotube (2012) J Lumin 132: 147-152. https://doi.org/10.1016/j.jlumin.2011.08.004
28. Jangu C, Savage AM, Zhang Z, Schultz AR, Madsen LA, et al. Sulfonimide-containing triblock copolymers for improved conductivity and mechanical performance (2015) Macromolecules 48: 4520-4528. https://doi.org/10.1021/acs.macromol.5b01009
29. Palli B and Padmanabhan V. Chain flexibility for tuning effective interactions in blends of polymers and polymer-grafted nanoparticles (2014) Soft Matter 10: 6777-6782. https://doi.org/10.1039/c4sm00991f
30. Rolland J, Poggi E, Vlad A and Gohy J. Single-ion diblock copolymers for solid-state polymer electrolytes (2015) Polymer (Guildf) 68: 344-352. https://doi.org/10.1016/j.polymer.2015.04.056
31. Oh H, Xu K, Yoo HD, Kim DS, Chanthad C, et al. Poly(arylene ether)-based single-ion conductors for lithium-ion batteries (2016) Chem Mater 28: 188-196. https://doi.org/10.1021/acs.chemmater.5b03735.s001
32. Rohan R, Pareek K, Chen Z, Cai W, Zhang Y, et al. A high performance polysiloxane-based single ion conducting polymeric electrolyte membrane for application in lithium ion batteries (2015) J Mater Chem A 3: 20267-20276. https://doi.org/10.1039/c5ta02628h
33. Kumar KA and Gowda DC. Reduction of aldehydes and ketones to corresponding alcohols using diammonium hydrogen phosphite and commercial zinc dust (2011) E-J Chem 8: 49-52. https://doi.org/10.1155/2011/493685
34. Chmielewska E and Kafarski P. Synthetic procedures leading towards Aminobisphosphonates (2016) Molecules 21: 1474. https://doi.org/10.3390/molecules21111474
35. Ghelichi M, Qazvini NT, Jafari SH, Khonakdar HA, Farajollahi Y, et al. Conformational, thermal, and ionic conductivity behavior of PEO in PEO/PMMA miscible blend : investigating the effect of lithium salt (2013) J App Poly Sci 129: 1868-1874. https://doi.org/10.1002/app.38897

Citation: Zhao W, Mei X, Yue Z and Mandal BK. Solid polymer electrolytes derived from oligomeric poly(ethylene oxide) chain-grafted crosslinked polystyrene microspheres (2020) Edelweiss Chem Sci J 3: 17-23.

36. Kuo C, Li W, Chen P, Liao JW, Tseng CG, et al. Effect of plasticizer and lithium salt concentration in PMMA-based composite polymer electrolytes (2013) Int J Electrochem Sci 8: 5007-5021.
37. Ahmad A, Rahman MYA, Low SP and Hamzah H. Effect of $LiBF_4$ salt concentration on the properties of plasticized MG49-TiO_2 based nanocomposite polymer electrolyte (2011) ISRN Mater Sci 2011: 1-7. https://doi.org/10.5402/2011/401280
38. Wetjen M, Kim GT, Joost M, Appetecchi GB, Winter M, et al Thermal and electrochemical properties of PEO-LiTFSI-Pyr_{14} TFSI-based composite cathodes, incorporating 4 V-class cathode active materials (2014) J Power Sources 246: 846-857. https://doi.org/10.1016/j.jpowsour.2013.08.037
39. Yang R, Zhang S, Zhang L and Liu W. Electrical properties of composite polymer electrolytes based on PEO-SN-$LiCF_3SO_3$ (2013) Int J Electrochem Sci 8: 10163-10169.
40. Tang C, Hackenberg K, Fu Q, Ajayan PM and Ardebili H. High ion conducting polymer nanocomposite electrolytes using hybrid nanofillers (2012) Nano Lett 12: 1152-1156. https://doi.org/10.1021/nl202692y
41. Zhao Y, Wu C, Peng G, Chen X, Yao X, et al. A new solid polymer electrolyte incorporating $Li_{10}GeP_2S_{12}$ into a polyethylene oxide matrix for all-solid-state lithium batteries (2016) J Power Sources 301: 47-53. https://doi.org/10.1016/j.jpowsour.2015.09.111
42. Masoud EM, El-Bellihi A-A, Bayoumy WA and Mousa MA. Organic-inorganic composite polymer electrolyte based on PEO-$LiClO_4$ and nano-Al_2O_3 filler for lithium polymer batteries: Dielectric and transport properties (2013) J Alloys Compd 575: 223-228. https://doi.org/10.1016/j.jallcom.2013.04.054
43. Ibrahim S and Johan MR. Thermolysis and conductivity studies of Poly(ethylene oxide) (PEO) based polymer electrolytes doped with carbon nanotube (2012) Int J Electrochem Sci 7: 2596-2615.